SUPPRESSION OF THE TRANSFORMER RATIO DUE TO DISTRIBUTED INJECTION OF ELECTRONS IN A PLASMA WAKEFIELD ACCELERATOR*

N. Vafaei-Najafabadi†, W. An, C.E. Clayton, C. Joshi, W. Lu‡, K.A. Marsh,
W.B. Mori, UCLA, Los Angeles, CA 90095, USA
E. Adli§, C.I. Clarke, S. Corde, J.-P. Delahaye, R.J. England, A.S. Fisher, J. Frederico, S.J. Gessner,
M.J. Hogan, S.Z. Li, M.D. Litos, D. Walz, Z. Wu, SLAC, Menlo Park, CA 94025, USA
P. Muggli, Max Planck Institute for Physics, Munich, Germany

Abstract

Evidence of beam loading due to distributed injection in Plasma Wakefield Accelerator experiments carried out at the FACET facility at SLAC during the year 2012 is presented. The source of the injected charge is tunnel ionization of Rb^+ inside the wake, which occurs along the length of the interaction at each minima of envelope betatron oscillation. Rb was used specifically to mitigate the problem of head erosion, which limited the energy gain in earlier experiments using Li that were carried out at FFTB in SLAC. In the present experiment however, electrons produced via secondary ionization of Rb were injected in the wake and led to a severe depletion of the accelerating wake, i.e. beam loading, which is observed as a reduction of mean, i.e. measured, transformer ratio. This "dark current" limitation on the maximum achievable accelerating gradient is also pertinent to other heavier ions that are potential candidates for high-gradient PWFA.

INTRODUCTION

A Plasma Wakefield Accelerator (PWFA) uses a short, dense, high current electron beam to drive a high amplitude wake [1], which can accelerate electrons with gradients that are orders of magnitude larger than the conventional accelerators [2]. When the beam density (n_b) is higher than the plasma density (n_p), the electron beam expels all of the plasma electrons locally and creates a blowout region, a structure of uniform ion density that accelerates and focuses electrons [3]. The FACET Facility at SLAC [4] is currently used for further research on PWFA.

Two particular physics problems that have to be addressed are the problems of head erosion [5] and ion motion [6]. Head erosion is a physical effect limiting the length of the acceleration. Briefly, if the plasma is generated by the beam via field ionization, as was the case in [2], the part of the beam that ionizes the medium into plasma is not in the blowout region and therefore continues to expand at a rate that is dependent on its emittance. The expansion then causes the ionization front to recede back in the frame of the beam. The rate of this "head erosion" effect is dependent on $1/\gamma$, ϵ_n, and $\mathrm{IP}^{1.73}$ [7], where ϵ_n is the normalized emittance and IP is the ionization potential of the element that is being ionized. Ion motion is a problem because it leads to distortion of the linear focusing force in the blowout regime, and it occurs for $n_b/n_p > m_i/m_e$.

Both of these problems can be addressed by switching Li (used previously [2]) to a higher Z element, such as Rb. With an ionization potential that is 23% smaller than Li, the application of the scaling equations for head erosion implies that the interaction length in Rb would be 40% longer, leading to a proportional increase in maximum achievable energy. Additionally, with an atomic mass of over 12 times larger than Li, Rb ions are an order of magnitude less mobile. On the other hand, the ionization potential of the second Li electron is so high (75.6 eV) that it is not exceeded during the experiment. This is not the case with Rb. The second ionization potential of Rb is 27.3 eV, which could be reached during the experiment. Here, we show that this secondary ionization of Rb is responsible for significantly reducing the energy gradient. The suppression of the accelerating gradient is diagnosed in this experiment by monitoring average transformer ratio $\langle T \rangle$, which can be measured in experiments as $\Delta W^+/\Delta W^- = \int E^+ dz / \int E^- dz$.

EXPERIMENTAL SETUP

The 3 nC, 20.35 GeV electron beam from the FACET facility at SLAC was focused on the rising edge of a column of Rb vapor at the neutral density of 2.7×10^{17} cm^{-3} in a heat pipe oven [8] (Fig. 1). Rb gas was contained in the oven using Ar as buffer. Therefore, the density of Ar rose as the density of Rb fell in such a way that the total pressure stayed the same. The bunch length of the beam was monitored for every shot using the integrated transition radiation signal, which was generated as the beam traversed a 1 μm thick Ti foil and was measured by a pyroelectric detector (pyro). This signal correlated with a THz Michelson interferometer (Fig. 1) and was the main diagnostic of the bunch length. Two absolutely calibrated toroids before and after

*The work at UCLA was supported by DOE grant DE-FG02-92-ER40727 and NSF grant PHY-0936266. The simulations were carried out on the Hoffman cluster at UCLA. Work at SLAC was supported by Department of Energy contract DE-AC02-7600515.

† navidvafa@ucla.edu
‡ Also at Tsinghua University, Beijing 100084, China
§ Also at Department of Physics, University of Oslo, 0316 Oslo, Norway

ISBN 978-3-95450-138-0

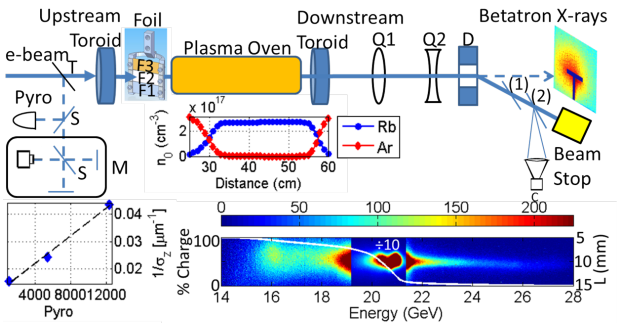

Figure 1: Experimental setup. The electron beam enters from the left. Transition radiation generated as the beam traverses the 1 μm Ti foil is observed simultaneously by a pyroelectric detector (Pyro) and a THz Michelson interferometer (M). Correlation of the two signals is shown beneath the setup. Foils can be inserted in the path of the beam before it enters the plasma oven to change its emittance from $\epsilon_{n0} = 250 \times 50\,\mu$m (see Table 1 for details). Underneath the schematic of the oven, the density profiles of neutral Rb and Ar are shown in blue circles and red diamonds, respectively. The quadrupole magnets Q1 and Q2 along with the dipole magnet D form the spectrometer. The Cherenkov radiation emitted between silicon wafers (1) and (2) is detected by camera C. An example of the energy spectrum with the white curve showing the integrated charge is shown below the camera C. The charge near 20.4 GeV observed not to lose any energy has been attenuated by a factor of 10. The Lanex screen, shielded by a 1mm copper foil, detects the betatron x-rays.

the plasma oven were used to monitor the incoming and outgoing charge. Excess charge generated during the interaction was calculated by subtracting the upstream toroid from the downstream one. To vary the beam emittance, a set of foils of various thicknesses and compositions (F1-F3, see Fig. 1 and Table 1) were placed in to path of the beam. An imaging spectrometer containing two quadrupole magnets and one dipole magnet are used to measure the energy spectrum of the beam after the plasma. After being dispersed by the dipole, the electrons traveled in air and generated Cherenkov radiation, which was imaged onto a 12 bit CCD. An example of such image is shown in Fig. 1. X-ray photons of 50-200 keV are observed using a Lanex film, which is shielded from low energy x-rays using a 1 mm copper mask [9].

Table 1: Composition, Thickness, and Emittance Contribution [10] of the Foils F1-F3 in Fig. 1

Foil	Thickness	Metal Composition	ϵ_n/ϵ_{n0}
F1	25.4 μm	71.15 Ag/28.1 Cu/0.75 Ni	1.2
F2	50.8 μm	25.57 Au/74.43 Cu	1.3
F3	38.1 μm	81.1 Au/16 Cu/2 Ni	1.4

METHODS AND ANALYSIS

The energy gain and energy loss are needed to calculate the average transformer ratio. To calculate these values, a plot of the integrated charge (white curve shown in spectrometer image in Fig. 1) is first produced by integrating the counts on the spectrometer image first in the non-dispersive dimension and then in the dispersive dimension. Energy gain and loss in this experiment are defined as the energies where this curve exceeds 2% and 98%, respectively. For example, in the spectrometer image shown in Fig. 1, the maximum energy is 24.4 GeV and minimum energy is 15.1 GeV, leading to values of 4 GeV and 5.3 GeV for energy gain (ΔW^+) and energy loss (ΔW^-), respectively.

From the same spectrometer image, it is clear that a significant portion of the charge has not moved from the initial energy. This portion of the beam is the unaffected charge and is dependent on where the ionization occurs in the frame of the beam. Modeling the ionization with the ADK model [11, 12], we can plot an ionization contour for the beam and calculate the amount of unaffected charge at a certain ionization contour based on the element and beam characteristics. This measurement can also be applied in reverse, inferring the initial size of the beam as it enters the plasma. The insertion of foils F1-F3 causes an increase in the beam size [13], reducing the beam density and field, leading to an increase in the unaffected charge for increasing foil number. Typical value of the unaffected charge as a function of total charge were 38% for the case of no foil, 43% for F1, 43% for F2 and 51% for F3. These values are for a pyro reading between 3000 and 6000 or $\sigma_z \sim 40\,\mu$m. Subtracting the unaffected charge from the total charge yields the amount of charge that participated in driving the wake and forming the accelerating structure.

Once the Rb vapor was ionized, the experiment quickly evolved into the blowout regime, where the electron beam traveled in a uniform ion column. The evolution of the electron beam in this ion cavity can be illustrated by the envelope evolution model [14]. If the initial beam radius is larger than the matched radius, given by $\sigma_r^2 = \epsilon_n(c/\omega_p)\sqrt{2/\gamma}$ [15], the envelope radius of the beam decreases in the up-ramp of the plasma and then oscillates along the entire length of the interaction. As the envelope of the beam oscillates, the electrons generate x-rays that will be observed by the x-ray diagnostic. To calculate the x-ray yield resulting only from the beam-plasma interaction, background data is obtained by sending the electron beam through neutral Ar. This yields a background emission region, which is independent of the plasma interaction, and is then selected and blocked in the experimental results. Furthermore, since the number of electrons participating in the oscillations varies from one experiment to another, the x-rays yield is normalized to the participating charge. In this manner, the x-ray yield per electron can be compared in different experiments.

The envelope oscillation of the beam has another signif-

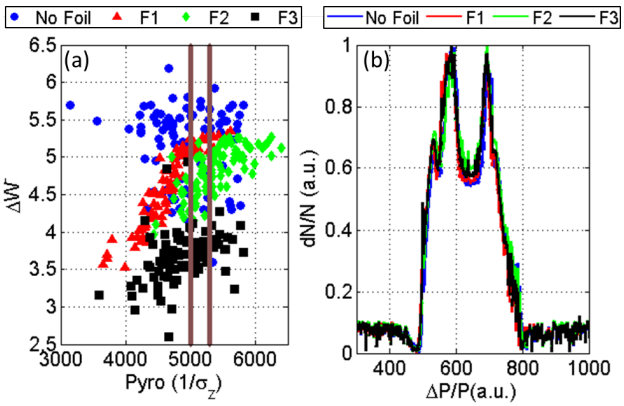

Figure 2: (a) Energy loss as a function of inverse bunch length ($\propto$ pyro). Data with 5000<pyro<5300 is marked. (b) Projection of phase space for data with 5000<pyro<5300. Current profiles are nearly identical.

icant consequence. As the envelope radius decreases, the radial electric field of the beam increases. For a participating charge of $N = 1.3 \times 10^{10}$ electrons, $\sigma_z = 40\,\mu$m and $\sigma_r^* = 3\,\mu$m, where σ_r^* represents the minimum value of the envelope radius, the electric field can be calculated from $E_r^{max} = 17.3\,\text{GV/m}(N/10^{10})(10\mu\text{m}/\sigma_r^*)(30\mu\text{m}/\sigma_z)$, which yields an E_r^{max} of 56 GV/m. The peak electric field strength required to ionize Rb^+ by 10% for the same σ_z is 53 GV/m. Therefore, Rb^+ electrons are ionized at the lowest point of the radius oscillation, released inside the wake, accelerated by the wake structure [14], and observed as excess charge on the toroids.

To minimize the effect that different current density profiles can have on the results, ΔW^-, ΔW^+, and excess charge data were filtered to a narrow range of pyro reading with nearly identical current densities (Fig. 2). This specific range of pyro (5000 <pyro< 5300) was selected because the data contained in this region spanned a large range of values. For instance, ΔW^- shown in Fig. 2(a) varied by more than a factor of 2. This variation allowed for meaningful study of the correlation between different parameters. The current density profiles were inferred from the projection of the electron beam's phase space, which is recorded on every shot. This projection is obtained using a vertical half period wiggler magnet, which reroutes electrons through two small bends [16]. The resulting radiation illuminates a scintillating crystal of YAG:Ce, which is imaged onto a CCD camera. These profiles confirm that experimental data points in the narrow range of pyro selected indeed have a beam current profile that is nearly identical to one another (Fig. 2(b)). Using this dataset selected for their similar current density profile, it is observed that excess charge is almost linearly correlated with both the x-ray yield and energy loss [17]. In other words, for every betatron oscillation contributing to x-ray yield, the excess charge increases as well. Furthermore, the correlation between excess charge and the energy loss strongly implies that this distributed trapping occurs over the length

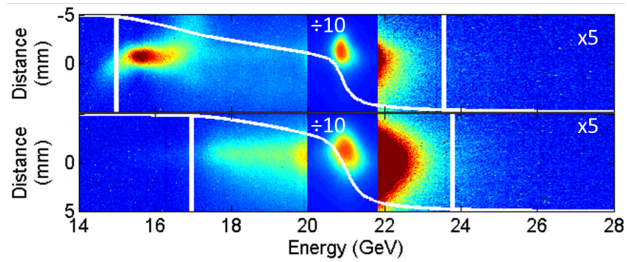

Figure 3: Electron energy spectra. Top: Excess charge was 770 pC and $\langle T \rangle = 0.6$. Bottom: Excess charge was 510 pC and $\langle T \rangle = 1.1$; Foil F3 was also inserted in the beam path. $\langle T \rangle$ decreases as the excess charge increases.

of the interaction. This distributed injection of charge in turn beam loads the wake, reducing the accelerating gradient and the transformer ratio. As stated earlier, this effect is observed in the experiment by measuring the average transformer ratio $\langle T \rangle$. The spectrum corresponding to the two data points with the highest and the lowest excess charge from the narrow range of pyro selected in Fig. 2 is shown in Fig. 3. It is evident that while the energy loss increases significantly, the energy gain is nearly the same between the two as the result of the heavy beam loading.

In summary, secondary ionization of heavy ion species in the blowout region is a significant limiting factor for the accelerating gradient in PWFA. In our experiment, Rb^+ ionization led to beam loading and a reduction in $\langle T \rangle$ by a factor of two. Other heavy elements considered as candidates to mitigate head erosion and ion motion in PWFA experiments may be limited in their accelerating gradient by the same effect.

REFERENCES

[1] P. Chen et al., Phys. Rev. Lett. 56 (1985) 693.
[2] I. Blumenfeld, et al., Nature 445 (2007) 741.
[3] W. Lu et al., Phys. Rev. Lett. 96 (2006) 165002.
[4] M. J. Hogan, et al., New J. Phys. 12 (2010) 055030.
[5] I. Blumenfeld, Ph.D. Thesis, Stanford University (2009)
[6] J. Rosenzweig et al., Phys Rev. Lett. 95 (2005) 195002
[7] M. Zhao, Ph.D. Thesis, UCLA (2008)
[8] P. Muggli, et al., IEEE T. Plasma. Sci. 27 (1999) 791.
[9] M. Litos and S. Corde, AAC'12, Austin, June 2012, p. 705.
[10] S. Li et al., AAC'12, Austin, June 2012, p. 1507.
[11] D. L. Bruhwiler et al., Phys. Plasmas 10 (2003) 2022.
[12] C. L. O'Connell et al., Phys. Rev. ST Accel. Beams 9 (2006) 101301.
[13] K. A. Marsh et al. NA-PAC'13, Pasadena, September 2013, TH0CA1
[14] E. Oz et al., Phys. Rev. Lett. 98 (2007) 084801.
[15] P. Muggli et al., Phys. Rev. Lett. 93 (2004) 014802.
[16] S. J. Gessner et al., IPAC'13, Shanghai, May 2013, TUPWA069, pp. 1865-1867
[17] Vafaei-Najafabadi, et al., submitted.

ISBN 978-3-95450-138-0